

Crystallizing proteins on the basis of their precipitation diagram determined using a microfluidic formulator

Morten O. A. Sommer* and Sine Larsen

Centre for Crystallographic Studies, Department of Chemistry, University of Copenhagen, Denmark.
E-mail: morten@ccs.ki.ku.dk

Crystallization of proteins from a purified protein solution remains a bottleneck in the structure determination pipeline. In this paper the crystallization problem is addressed using a microfluidic device capable of determining detailed protein precipitation diagrams using less than 10 μL of protein sample. Based on the experimentally determined protein phase behavior, a crystallization screen can be designed to accommodate the physical chemistry of the particular protein target. Such a tailor-made crystallization screen has a high probability of yielding crystallization hits. The approach is applied to two different proteins: the calcium pump (SERCA), an eukaryotic integral membrane protein, and UMP kinase, a prokaryotic soluble kinase. Protein phase behavior is mapped for both proteins and tailor-made crystallization screens are designed for the two proteins resulting in about 50% crystallization probability per experiment. This illustrates the power of using microfluidic devices for detailed characterization of protein phase behavior prior to crystallization trials.

1. Introduction

Recent years have seen an increasing interest in elucidating the full proteome of various organisms leading to the founding of several structural genomics consortia. The large-scale structural determination effort has brought about an intensive development of high-throughput technologies for all steps leading to the determination of macromolecular structure, and the structural genomics consortia have proven successful in determining the structure of several smaller soluble proteins. However, large-scale structural determination of more challenging projects such as integral membrane proteins and large macromolecular complexes remain to be seen.

One of the main bottlenecks in the structure determination of these challenging targets is obtaining diffraction-quality crystals (Chayen, 2003). The common approach to the crystallization problem of large-scale crystallization facilities is the utilization of commercial sparse matrix screens, consisting of solutions previously identified as successful crystallizing agents (Carter & Carter, 1979; Jancarik & Kim, 1991). However, proteins exhibit complex and diverse physical chemistry, which may be different from the physical chemistry exhibited by the subset of proteins which the sparse matrix screens are based on; hence, not all proteins are likely to crystallize using sparse matrix approaches. In these cases a

different approach is required, taking into account the phase behavior of the particular protein target. Characterization of protein solubility has previously been used to individualize crystallization trials by adjusting protein concentration before setting up crystallization experiments (Stura *et al.*, 1992); automated microbatch experiments have been used for detailed grid screening for a particular protein–precipitant pair followed by subsequent crystallization based on the determined phase diagram (Saridakis *et al.*, 1994); and microdispensing techniques have been used for mapping of protein solubility under a few chemical conditions leading to successful identification of crystallization conditions (Santesson *et al.*, 2003).

An optimal crystallization screen for the specific protein can be devised if detailed knowledge of the protein phase behavior is available. However, if the screen should include several different chemical conditions it would require thousands of chemical experiments to be performed prior to setting up the crystallization experiments, consuming large amounts of protein using conventional techniques. Using a microfluidic formulation device, rapid large-scale mapping of the protein phase behavior was recently performed for the model protein xylanase leading to the design of a crystallization screen with a high crystallization hit rate compared with commercial sparse matrix screens (Hansen, Sommer & Quake, 2004).

In this paper, results are presented which describe the utilization of the microfluidic formulation device designed by Hansen, Sommer & Quake (2004) for systematic mapping of the phase behavior of two non-trivial protein targets: UMP kinase from *Sulfolobus solfataricus*, a soluble prokaryotic kinase, and Ca^{2+} ATPase, an eukaryotic integral membrane protein, which has been previously crystallized (Toyoshima *et al.*, 2000; Toyoshima & Nomura, 2002; Sørensen *et al.*, 2004). Based on the experimentally determined phase behavior, tailor-made crystallization screens are produced identifying several crystallization conditions for both targets. This approach to the crystallization problem is based on the basic physical chemistry of protein phase behavior and may prove useful to implement in large-scale facilities working on protein targets exhibiting non-trivial phase behavior.

2. Crystallization of proteins based on their phase behavior

The starting point for a crystallization trial is an undersaturated solution of purified protein. To grow a protein crystal from the solution requires the manipulation of the physical and chemical parameters governing the system to create a solution that is supersaturated with respect to the protein. From a supersaturated solution a solid phase will nucleate and grow until the chemical potentials of the protein molecules in the two phases are equal. Whether nucleation is described best by classical homogeneous nucleation models (Garcia-Ruiz, 2003; Zhang & Liu, 2004) or by heterogeneous nucleation models (Cacciuto *et al.*, 2004), the nucleation frequency is highly dependent on the protein saturation, defined as the ratio of the actual protein concentration in solution to the thermodynamic protein solubility. When the protein saturation is above 1, the solution is supersaturated. At low supersaturation, critical nuclei are not likely to form owing to high nucleation energy barriers; however, if a critical nucleus is supplied to solution at low supersaturation it may enter the growth phase and turn into a crystal of appreciable size (Saridakis & Chayen, 2003). As supersaturation increases, the nucleation frequency is drastically increased and many nuclei are formed resulting in a competition for free protein molecules between the independent nuclei; in this case none of the nuclei are likely to grow to an appreciable size and the result will be rapid precipitation of the protein. The protein concentration at which nucleation is an instantaneous event resulting in rapid precipitation is termed the supersolubility limit. Plotting the protein solubility and supersolubility as a function of a physical or chemical parameter such as temperature, salt concentration, polymer concentration or pH gives rise to a protein phase diagram (Fig. 1).

In order to crystallize a protein from solution it is necessary to change the physical chemical state of the system so formation of a few critical nuclei is favored followed by the ordered addition of protein growth units (McPherson, 1999). Formation of critical nuclei requires that the protein concentration is above the solubility limit and ordered addition of protein growth units is most likely to occur when the protein

concentration is below the supersolubility limit. The region of phase space situated between the solubility boundary and the supersolubility boundary is termed the metastable region (Garcia-Ruiz, 2003). Focusing crystallization experiments to this region would increase the probability of successfully crystallizing the protein, since the region of protein phase space which is conducive to crystallization is most likely to be situated between the solubility boundary and the supersolubility boundary even though crystals can also grow from precipitate.

The region conducive to crystallization may be large, which is the case for the protein hen egg-white lysozyme, resulting in a relatively straightforward crystallization and a high tolerance regarding variation of the critical parameters influencing protein crystallization. Proteins with large metastable regions are likely to be crystallized using sparse matrix approaches, since it is not critical to have all parameters adjusted correctly. However, if the region conducive to crystallization is small, little variation in the parameters affecting the crystallization process can be tolerated. In this case, sparse matrix screens are not likely to identify crystallization conditions and end up being a search for a needle in a haystack. In these cases a method is needed to identify potential crystallization conditions in a more systematic way.

3. Microfluidics and protein crystallization

The development of multilayer soft lithography (MSL) (Unger *et al.*, 2000) has proven critical in developing viable microfluidic devices for biological applications such as cell biology (Thorsen *et al.*, 2002), polymerase chain reaction (Liu *et al.*, 2003) and DNA purification (Hong *et al.*, 2004). Microfluidic devices for protein crystallization were pioneered by the development of micro free interface diffusion (μ FID)

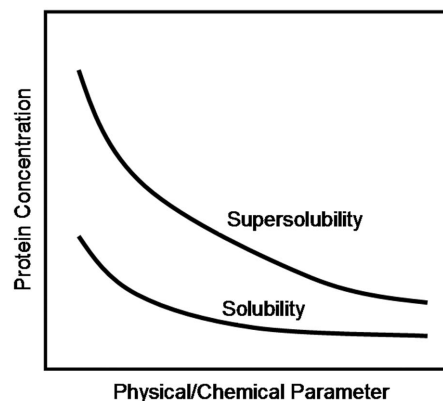


Figure 1 Generic protein phase diagram. Protein solubility and supersolubility vary as a function of a physical parameter such as temperature or a chemical parameter such as salt concentration or pH. Clearly, crystallization of the protein will not occur in the region of phase space below the solubility limit but from a supersaturated solution. However, if protein precipitates rapidly, large single crystals are not likely to form from the precipitate; hence, crystallization experiments should be designed to equilibrate in the metastable region above the solubility limit and below the supersolubility limit.

(Hansen *et al.*, 2002; Hansen & Quake, 2003; Hansen, Sommer, Self *et al.*, 2004). μ FID miniaturized conventional counter-diffusion techniques resulting in a lower sample consumption and increased throughput owing to the ability to perform many experiments in parallel. Even more interesting is its increased crystallization hit rate owing to the well controlled mixing kinetics (Hansen, Sommer, Self *et al.*, 2004) and a favorable fluidic micro-environment (Hansen & Quake, 2003).

Another application of microfluidics to protein crystallization uses a two-phase flow (Thorsen *et al.*, 2001; Tice *et al.*, 2003) to generate water droplets immersed in oil inside microfluidic channels. The composition of these droplets can be actively controlled from a subset of three solutions enabling rapid generation of crystallization experiments (Zheng *et al.*, 2003). Loading experiments from the chip onto a thin glass capillary enables screening of crystal diffraction quality using synchrotron radiation (Zheng *et al.*, 2004).

Common for these microfluidic developments is that the crystallization problem is handled in much the same way as previously. μ FID utilizes sparse matrix screens and the two-phase flow devices are very similar to the well known grid screen for a particular chemical condition. However, recently MSL has been used to design and fabricate a microfluidic formulation device with the ability to meter solutions of varying physical properties in 80 pL increments into a 5 nL reaction chamber followed by rapid active mixing (Hansen, Sommer & Quake, 2004). The device can generate complex mixtures of 32 stock solutions with high accuracy in the 5 nL reaction chamber enabling detailed investigation of protein phase behavior using small amounts of protein sample. The device was used to identify chemical conditions promoting precipitation of the 21 kDa protein endo-1,4- β -xylanase from *T. reesei*. For each of the identified precipitating chemicals the supersolubility limit was mapped out giving rise to several protein precipitation diagrams. These precipitation diagrams formed the basis for setting up a rational crystallization screen based on the physical chemistry of the particular protein. Comparing the crystallization hit rate of the rational physics-based screen and commercially available sparse matrix screens showed that the physics-based screen had a 72-fold higher crystallization hit rate (Hansen, Sommer & Quake, 2004), illustrating the power of detailed characterization of protein phase behavior prior to setting up crystallization experiments. This approach individualizes the crystallization process from the very first crystallization experiments, and the initial crystallization screen is based on the phase behavior of the specific protein target.

This paper presents results of the physics-based approach applied to both the calcium pump [sarco(endo)plasmic reticulum Ca^{2+} adenosine triphosphatase (SERCA), which is an integral membrane protein] and to the soluble protein UMP kinase using the microfluidic formulation device (Hansen, Sommer & Quake, 2004). The results obtained highlight the power of using microfluidics for supersolubility screening for identification of crystallization conditions.

4. Crystallizing the eukaryotic integral membrane protein SERCA

Membrane proteins have proven rather difficult to crystallize. This can be attributed to their complex physical chemistry, low availability and the fact that the commercial sparse matrix screens do not seem to work very well for many membrane proteins. In order to test the feasibility of the physics-based approach for membrane proteins, SERCA was used as a model protein since it has previously been crystallized (Toyoshima *et al.*, 2000; Toyoshima & Nomura, 2002; Sørensen *et al.*, 2004) and reliable purification methods are established (Møller *et al.*, 2002).

SERCA is a 110 kDa integral membrane protein purified from rabbit fast-twitch muscle according to procedures described by Møller *et al.* (2002) and Sørensen *et al.* (2004). The protein concentration was 12 mg ml⁻¹, 30 mM C12E8 was used as detergent and the protein buffer contained 100 mM MOPS pH 6.8, 80 mM potassium chloride, 10 mM calcium chloride, 3 mM magnesium chloride, 1 mM AMPPCP and 20% v/v glycerol. The protein sample was centrifuged for 1 h at 50.000 g at 277 K to spin down any aggregates before loading the microfluidic formulation device.

4.1. Precipitant screen

The first step of the microfluidic precipitation analysis is to identify precipitating chemical conditions. The microfluidic formulator was loaded with 13 different salt solutions and four different polyethylene glycol (PEG) solutions, glycerol and a linear buffer system (Newman, 2004). Protein precipitation was screened for each of the salts in various combinations with glycerol and different molecular-weight PEGs. For each salt the following 19 different chemical conditions were screened: 70% salt stock solution; 50% salt stock solution and 8% v/v glycerol; 50% salt stock solution and 5% w/v PEG 400, 1500, 4000 and 8000; 5% salt stock solution and 40% v/v glycerol; 5% salt stock solution and 25% w/v PEG 400, 1500, 4000 and 8000; 5% salt stock solution, 8% v/v glycerol and 25% w/v PEG 400, 1500, 4000 and 8000; 5% salt stock solution, 40% v/v glycerol and 5% w/v PEG 400, 1500, 4000 and 8000. In total, SERCA phase behavior was screened for 247 unique chemical conditions at three different protein concentrations (0.72 mg ml⁻¹, 2.4 mg ml⁻¹ and 4.8 mg ml⁻¹). The screen consumed less than 1 μ L of protein sample.

Every mixture was automatically evaluated to be either precipitated or clear. Automatic categorization of precipitated or clear drops was performed by taking a digital picture of a segment of the reaction chamber before and after addition of protein. Calculating the standard deviation of the intensity of pixels (SDIP) for both pictures and subtracting the SDIP before addition of protein from the SDIP after addition of protein gave a reliable measure of protein-induced precipitation.

The screen allowed a ranking of the chemical conditions in terms of their ability to precipitate SERCA. If a chemical condition precipitated the protein at 0.72 mg ml⁻¹, 2.4 mg ml⁻¹, 4.8 mg ml⁻¹ or not at all, the chemical condition

was classified as a strong precipitant, medium precipitant, weak precipitant or non-precipitating condition, respectively. 78 of the 247 chemical conditions investigated were classified as strong precipitants, 38 chemical conditions were medium precipitants, 22 were weak precipitants and 107 were non-precipitating conditions. This classification of the chemical conditions allowed an ordering of each individual component making up the chemical conditions in terms of its ability to precipitate SERCA relative to its concentration (Fig. 2). Such an ordering of the precipitating strength of salts can illuminate specific interactions of particular salts and the protein. It is interesting to note that sodium acetate is rated the strongest precipitating salt, since sodium acetate has previously been used to crystallize SERCA (Sørensen *et al.*, 2004), indicating that strong precipitants may be particularly useful in crystallization trials for this protein.

4.2. SERCA phase behavior mapping

Based on the precipitant screen, 15 chemical conditions were selected for detailed mapping of SERCA phase behavior. The chemical conditions were selected to include salt additives of high, medium and low precipitant strength in combination with various PEGs and glycerol. The concentration of salt, PEG and glycerol were adjusted such that the average solubility of SERCA was between 0.5 and 2 mg ml⁻¹. Each precipitation diagram consisted of 42 independent experiments and consumed about 30 nL of protein sample.

The precipitation diagram of SERCA and PEG 1500 with glycerol and calcium acetate is shown in Fig. 3(a). SERCA

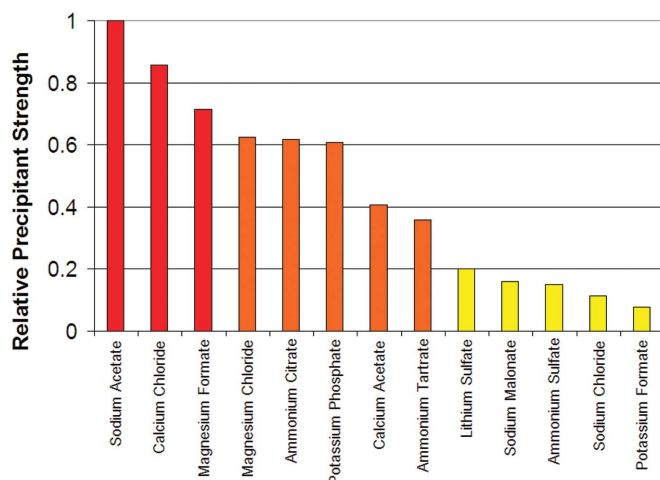


Figure 2

Precipitant strength of the individual salts for SERCA. The individual salts were each included under many chemical conditions in the precipitant screen conducted for SERCA. Each chemical condition was rated as strong (three points), medium (two points), weak (one point) or non-precipitant (zero points) depending on what protein concentration was needed to precipitate the solution. For each salt, points awarded to the chemical conditions containing that salt were averaged and then divided by the molar concentration of the salt stock solution. This resulted in an ordering of the salts in terms of their molar precipitating strength. Sodium acetate turned out to be the strongest precipitant for SERCA, which is interesting since sodium acetate has previously been used as a crystallization agent for SERCA (Sørensen *et al.*, 2004).

supersolubility does not vary significantly with PEG 1500 concentration, implying that the physical chemistry of the protein is dominated by effects of the additives glycerol and calcium acetate. The precipitation diagram of SERCA and PEG 1500 with potassium phosphate substituted for calcium acetate is seen in Fig. 3(b). SERCA supersolubility depends critically on PEG 1500 concentration in this case. Thus changing the additive from calcium acetate to potassium phosphate has a pronounced effect on the SERCA phase behavior indicating a specific interaction between SERCA and calcium acetate. It is interesting that the identity of a salt additive can substantially alter the protein phase behavior even though the salt additive does not have a high precipitant strength. This highlights that the precipitant strength is not the only parameter useful in determining the significance of a precipitant protein interaction.

4.3. Crystallization screen for SERCA based on experimentally determined phase behavior

Information about the supersolubility of SERCA enables a series of sitting-drop vapor diffusion crystallization experiments to be set up, equilibrating near the supersolubility limit as outlined in Fig. 3. Thus, each individual experiment has a maximum likelihood of crystallizing, since the experiment takes a path through the metastable region during equilibration towards the supersolubility limit. This is ensured for all crystallization experiments, since the specific interaction between a particular additive and the protein are known from the precipitation diagrams.

Based on 11 precipitation diagrams, 26 sitting-drop crystallization experiments (2 μ L + 2 μ L) equilibrating near the supersolubility limit were set up. The crystallization experiments were stored at 298 K for one week. Inspection of the experiments showed that eight conditions had small (10–50 μ m) thin plate clusters or rods often adjacent to phase separation, seven conditions had microcrystals, nine conditions had amorphous precipitate and three conditions were clear.

Thorough characterization of protein phase behavior was carried out for the integral membrane protein SERCA using less than 5 μ L of protein stock solution. This characterization allowed for evaluation of the precipitating strength of the chemicals used. It turned out that the salt with the highest precipitant strength, sodium acetate, had previously crystallized SERCA, indicating that an additive of a strong precipitant may be useful to crystallize SERCA, which was seen in the crystallization experiments where both sodium acetate and calcium chloride crystallized SERCA. Furthermore, the precipitation diagrams identified a salt additive with medium precipitant strength, calcium acetate, having a pronounced effect on the SERCA phase behavior (Fig. 3). Crystallization experiments set up based on the precipitation diagrams of SERCA resulted in a 58% crystallization hit rate identifying 15 conditions, which can be further optimized to obtain large crystals for diffraction studies.

5. Crystallizing the prokaryotic kinase UMP kinase

UMP kinase is a soluble prokaryotic protein of molecular weight 25 kDa. The protein was purified from *Sulfolobus solfataricus* and was in a buffer containing 10 mM TRIS pH 7.6 and 2 mM UMP. The protein was centrifuged at 20,000 g for 15 min at 277 K to spin down any aggregates prior to loading the microfluidic device.

5.1. Rational approach for crystallizing UMP kinase

The precipitation screen for UMP kinase consisted of 200 different chemical conditions each buffered at pH 4, 6 and 8 leading to a total of 600 chemical conditions. All conditions were tested for precipitation at 1.6 mg ml⁻¹ protein concentration. The sparse screen consumed less than 5 μ L of UMP kinase solution. Half of the chemical conditions investigated

precipitated UMP kinase; however, it was observed that the strongest precipitants were divalent salts in combination with PEG 4000 and PEG 8000 at pH 4 and 6.

Eight chemical conditions were identified as very strong precipitants and UMP kinase phase behavior was mapped for these precipitants. Each precipitation diagram consumed 100 nL of UMP kinase stock solution. Examples of precipitation diagrams for UMP kinase are shown in Fig. 4.

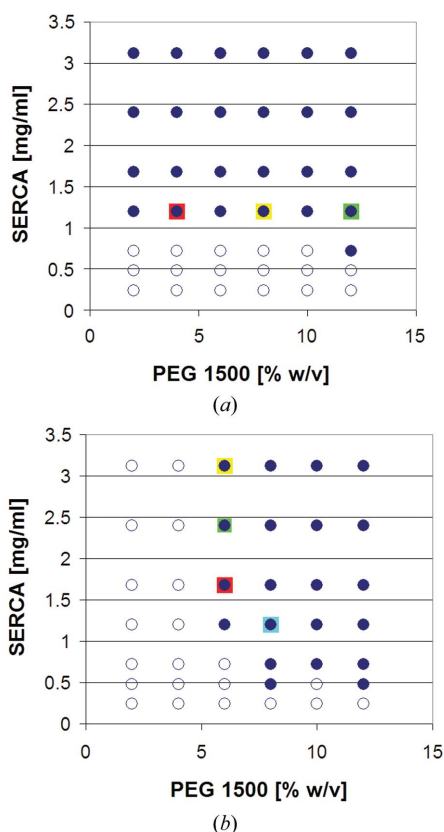


Figure 3

SERCA phase behavior. Filled circles correspond to precipitated conditions and open circles correspond to non-precipitating conditions. (a) Phase behavior of SERCA as a function of PEG 1500 concentration with 0.1 M 1:2:2 malic acid, MES, TRIS linear buffer pH 6.5 (Newman, 2004), 0.1 M calcium acetate and 8% v/v glycerol. The colored squares are the points in the phase diagram where sitting-drop experiments were intended to equilibrate. The experiments represented by the red and yellow squares resulted in small rod-shaped crystals emanating from phase separation; those represented by the green square gave thin plates clusters. (b) Phase behavior of SERCA as a function of PEG 1500 concentration with 0.1 M 1:2:2 malic acid, MES, TRIS linear buffer pH 6.5, 0.1 M potassium phosphate and 8% v/v glycerol. Sitting-drop crystallization experiment equilibration points are represented by the colored squares: the experiment represented by the yellow square remained clear, microcrystals and thin plates grew from the experiments represented by the green and red squares, and the experiment represented by the turquoise square resulted in amorphous precipitation.

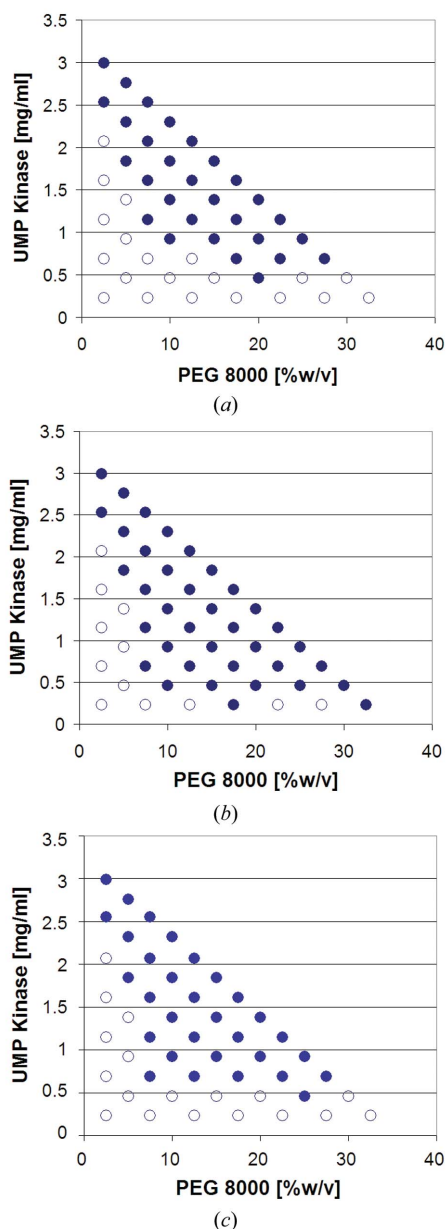


Figure 4

Effect of pH on phase behavior of UMP kinase. Filled circles correspond to precipitated conditions and open circles correspond to non-precipitating conditions. (a) Precipitation diagram for UMP kinase and PEG 8000 at pH 4 with 0.1 M 1:2:2 malic acid, MES, TRIS linear buffer and 50 mM magnesium formate. (b) Precipitation diagram for UMP kinase and PEG 8000 at pH 5 with 0.1 M 1:2:2 malic acid, MES, TRIS linear buffer and 50 mM magnesium formate. (c) Precipitation diagram for UMP kinase and PEG 8000 at pH 6 with 0.1 M 1:2:2 malic acid, MES, TRIS linear buffer and 50 mM magnesium formate.

Based on the precipitation diagrams, a crystallization screen consisting of 22 experiments was designed and set up as 2 μL + 2 μL sitting-drop crystallization experiments. The screen identified eight conditions as crystallization conditions with crystals of sizes between 20 and 100 μm , two conditions gave rise to microcrystals, six conditions were precipitated and six were clear; thus 45% of the crystallization experiments gave rise to crystalline material.

In order to investigate the possibility of optimizing crystallization conditions to give larger single crystals using protein phase behavior information, the precipitation diagram of one of the promising crystallization conditions (PEG 8000, 50 mM magnesium formate and 0.1 M MES buffer pH 6) was mapped for different pH values (Fig. 4). It was seen that UMP kinase was least soluble at pH 5 which indicates that at pH 5 the interactions between the protein molecules favor the precipitated phase the most. This variation of solubility with pH may be due to electrostatic effects from the surface charges of UMP kinase (theoretical isoelectric point 5.9). One would expect that larger crystals may form at the pH value with lowest protein solubility, since this may be a result of strong attractive interactions between the protein molecules. To investigate whether this feature of UMP kinase phase behavior could be useful as a guideline for optimizing crystallization conditions, experiments were set up equilibrating

on the supersolubility boundary at pH 4, 5 and 6. A relation between crystal morphology and pH was indicated in the experiments. It was observed that the crystals at pH 4 were rod-shaped, crystals at pH 5 were fewer with rectangular morphology and crystals at pH 6 were generally smaller (Fig. 5).

Characterization of the solubility of UMP kinase was carried out using a microfluidic formulation device using less than 10 μL of stock solution. Based on this solubility characterization a crystallization screen was designed for UMP kinase having a 45% crystallization hit rate. For one of the crystallization conditions an optimization procedure was attempted based on the idea that better crystals would grow at the pH value where the protein was least soluble. Even though results are not clear cut, crystal quality was improved by transferring crystallization conditions to different pH.

6. Conclusions

In this paper, use of a microfluidic device for detailed investigation of protein phase behavior of an integral membrane protein and a soluble kinase is presented. This knowledge was used to design tailor-made crystallization screens for the two proteins resulting in crystallization hit rates around 50%. The mapping of protein phase behavior required less than 10 μL of protein stock solution owing to the accurate fluid handling provided by the microfluidic formulation device. The presented results show that it is now feasible to have a case-specific approach to protein crystallization based on the physical chemistry of the particular protein target. Implementation of this type of microfluidic technology and method at larger crystallization facilities may help speed up structural genomics efforts on the challenging targets.

We acknowledge Professor Stephen R. Quake and Assistant Professor Carl Hansen for being very generous in helping with the implementation of the microfluidic platform at the Centre for Crystallographic Studies. Jens-Christian Navarro Poulsen is acknowledged for many good ideas and discussions and for assistance in the laboratory. We acknowledge Associate Professor Jörg Kutter and Detlef Snakenborg from MIC at the Danish Technical University for assistance with clean room fabrication and helpful discussions. We acknowledge Associate Professor Poul Nissen from the Department of Molecular Biology at Århus University and Professor Jesper Vuust Møller from the Department of Biophysics at Århus University for providing the SERCA protein sample. We acknowledge Assistant Professor Eva Johansson from the Centre for Crystallographic Studies and Professor Kaj Frank Jensen and Kristine Steen Jensen from the Department of Molecular Biology at the University of Copenhagen for providing the UMP kinase protein sample. Dorthe Boelskifte is acknowledged for setting up the crystallization experiments and Professor Jens Als-Nielsen is thanked for fruitful discussions.

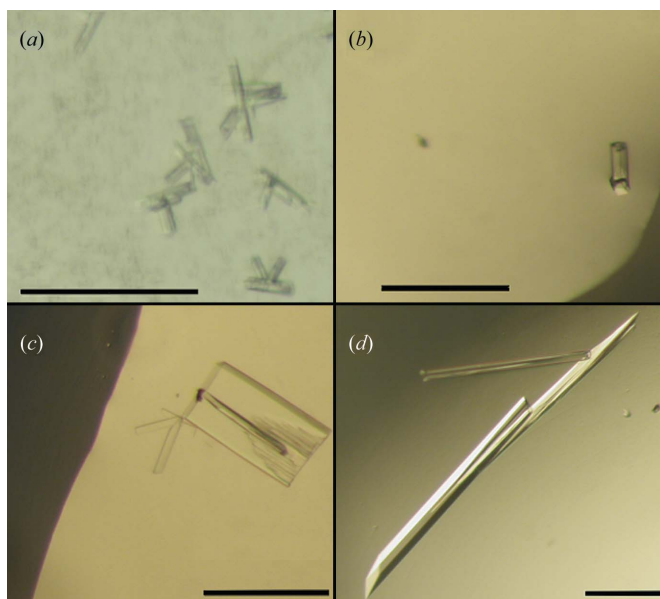


Figure 5

Effect of pH on crystal morphology of UMP kinase. The scale bar is 200 μm on all pictures. (a) Initial crystal hit, crystals grown from 0.8 mg ml^{-1} UMP K and 12.5% w/v PEG 8000 with 0.1 M MES pH 6 and 50 mM magnesium formate. (b) Small rectangular crystal grown at pH 6 in the presence of 1 mg ml^{-1} UMP K and 7.5% w/v PEG 8000 with 0.1 M 1:2:2 malic acid, MES, TRIS linear buffer and 50 mM magnesium formate. (c) Rectangular crystal and rod-shaped crystals grown at pH 5 in the presence of 0.7 mg ml^{-1} UMP K and 7.5% w/v PEG 8000 with 0.1 M 1:2:2 malic acid, MES, TRIS linear buffer and 50 mM magnesium formate. (d) Rod-shaped crystal grown at pH 4 in the presence of 1 mg ml^{-1} UMP K and 10% w/v PEG 8000 with 0.1 M 1:2:2 malic acid, MES, TRIS linear buffer and 50 mM magnesium formate.

References

- Cacciuto, A., Auer, S. & Frenkel, D. (2004). *Nature (London)*, **428**, 404–406.
- Carter, C. W. & Carter, C. W. (1979). *J. Biol. Chem.* **254**, 2219–2223.
- Chayen, N. E. (2003). *J. Struct. Funct. Genomics*, **4**, 115–120.
- Garcia-Ruiz, R. M. (2003). *J. Struct. Biol.* **142**, 22–31.
- Hansen, C. L. & Quake, S. R. (2003). *Curr. Opin. Struct. Biol.* **13**, 538–544.
- Hansen, C. L., Skordalakes, E., Berger, J. M. & Quake, S. R. (2002). *Proc. Natl. Acad. Sci. USA*, **99**, 16531–16536.
- Hansen, C. L., Sommer, M. O. A. & Quake, S. R. (2004). *Proc. Natl. Acad. Sci. USA*, **101**, 14431–14436.
- Hansen, C. L., Sommer, M. O. A., Self, K., Berger, J. M. & Quake, S. R. (2004). *Protein Crystallography in Drug Discovery*, edited by R. E. Babine and S. S. Abdel-Meguid, pp. 235–255. Weinheim: Wiley-VCH.
- Hong, J. W., Studer, V., Hang, G., French Anderson, W. & Quake, S. R. (2004). *Nature Biotechnol.* **22**, 435–439.
- Jancarik, J. & Kim, S. H. (1991). *J. Appl. Cryst.* **24**, 409–411.
- Liu, J., Hansen, C. L. & Quake, S. R. (2003). *Anal. Chem.* **75**, 4718–4723.
- McPherson, A. (1999). *Crystallization of Biological Macromolecules*. New York: Cold Spring Harbor Laboratory Press.
- Møller, J. V., Lenoir, G., Marchand, C., Montigny, C., leMaire, M., Toyoshima, C., Juul, B. S. & Champeil, P. (2002). *J. Biol. Chem.* **277**, 38647–38659.
- Newman, J. (2004). *Acta Cryst. D* **60**, 610–612.
- Santesson, S., Cedergren-Zeppezauer, E. S., Johansson, T., Laurell, T., Nilsson, J. & Nilsson, S. (2003). *Anal. Chem.* **75**, 1733–1740.
- Saridakis, E. & Chayen, N. E. (2003). *Biophys. J.* **84**, 1218–1222.
- Saridakis, E. G., Stewart, P. D. S., Lloyd, L. F. & Blow, D. M. (1994). *Acta Cryst. D* **50**, 293–297.
- Sørensen, T. L. M., Møller, J. V. & Nissen, P. (2004). *Science*, **304**, 1672–1675.
- Stura, E. A., Nemerow, G. R. & Wilson, I. A. (1992). *J. Cryst. Growth*, **122**, 273–285.
- Thorsen, T., Mearkl, S. & Quake, S. R. (2002). *Science*, **298**, 580–583.
- Thorsen, T., Roberts, R. W., Arnold, F. H. & Quake, S. R. (2001). *Phys. Rev. Lett.* **86**, 4163–4166.
- Tice, J. D., Song, H., Lyon, A. D. & Ismagilov, R. F. (2003). *Langmuir*, **19**, 9127–9133.
- Toyoshima, C., Nakasako, M., Nomura, H. & Ogawa, H. (2000). *Nature (London)*, **405**, 647–655.
- Toyoshima, C. & Nomura, H. (2002). *Nature (London)*, **418**, 605–611.
- Unger, M. A., Chou, H.-P., Thorsen, T., Scherer, A. & Quake, S. R. (2000). *Science*, **288**, 113–116.
- Zhang, K.-Q. & Liu, X. Y. (2004). *Nature (London)*, **429**, 739–743.
- Zheng, B., Roach, L. S. & Ismagilov, R. F. (2003). *J. Am. Chem. Soc.* **125**, 11170–11171.
- Zheng, B., Tice, J. D., Roach, L. S. & Ismagilov, R. F. (2004). *Angew. Chem. Int. Ed.* **43**, 2508–2511.